Atmos. Meas. Tech., 18, 4087–4102, 2025
https://doi.org/10.5194/amt-18-4087-2025

Atmospheric Measurement Techniques
Open Access
EGU

Vertical distribution of halogenated trace gases in the summer Arctic stratosphere based on two independent air sampling methods

Johannes C. Laube[1,2], Tanja J. Schuck[3], Sophie Baartman[4], Huilin Chen[5], Markus Geldenhuys[6,7], Steven van Heuven[5], Timo Keber[3], Maria Elena Popa[8], Elinor Tuffnell[2], Florian Voet[1], Bärbel Vogel[1], Thomas Wagenhäuser[3], Alessandro Zanchetta[5], and Andreas Engel[3]

[1]Institute of Climate and Energy Systems (ICE-4: Stratosphere), Forschungszentrum Jülich, Jülich, 52425, Germany
[2]School of Environmental Sciences, University of East Anglia, Norwich, NR4 7TJ, United Kingdom
[3]Institute for Atmospheric and Environmental Sciences, University of Frankfurt, Frankfurt (Main), 60438, Germany
[4]Meteorology and Air Quality group, Wageningen University and Research (WUR), P.O. Box 47, 6700 AA, Wageningen, the Netherlands
[5]Centre for Isotope Research, University of Groningen, Groningen, the Netherlands
[6]South African Weather Service, 1263 Heuwel Road, Centurion, South Africa
[7]Institute for Coastal and Marine Research, Nelson Mandela University, Gqeberha, 6001, South Africa
[8]Institute for Marine and Atmospheric Research Utrecht, Utrecht University, Utrecht, the Netherlands

Correspondence: Johannes C. Laube (j.laube@fz-juelich.de)

Received: 19 December 2024 – Discussion started: 10 January 2025
Revised: 16 May 2025 – Accepted: 20 May 2025 – Published: 29 August 2025

Abstract. Many halogenated trace gases are important greenhouse gases and/or contribute to stratospheric ozone depletion, yet their spatial distribution and temporal evolution in the stratosphere remain poorly constrained. We here present a new high-altitude dataset of a large range of these gases. The results are based on a large balloon flight in the Arctic in summer 2021. Air samples were collected using a passive (AirCore) as well as an active (cryogenic) technique; the former being the largest AirCore flown to date, thus enabling the quantification of an expanded variety of halogenated gases. The evaluation of the results demonstrates good comparability in most cases, but also revealed strengths and weaknesses for both sampler types. In addition, we show examples of the scientific value of this data, including the identification of air masses likely originating from the Asian Monsoon region, and the derivation of the average stratospheric transit times (i.e., the mean ages of air) from multiple tracers.

1 Introduction

Due to the ongoing effects of their decomposition products on the stratospheric ozone layer, the quantification of Ozone Depleting Substances (ODSs) remains important. This has recently been reemphasised as multiple ODSs have been found to either not decrease in global abundances as expected, or even increase (Vollmer et al., 2021; WMO, 2022; Western et al., 2022, 2023). In addition, many of these species – including related non-ODS fluorinated compounds – are strong greenhouse gases and have atmospheric lifetimes on the order of decades to millennia, with emissions therefore creating a long-lasting legacy in the atmosphere (Droste et al., 2020; Simmonds et al., 2020; Stanley et al., 2020; Say et al., 2021). While even the near-ground observations are unable to constrain the regional sources of global emissions for many halogenated species (Weiss et al., 2021), the data sparsity is distinctly more pronounced at the hard-to-reach stratospheric altitudes. Satellite data can offer good quality, but only for some species over certain altitude ranges (Stiller et al., 2012; Kolonjari et al., 2024; Saunders et al., 2025), with some products exhibiting higher uncertainties (Harrison et

al., 2012) or obvious biases (Dodangodage et al., 2021). Here we present a unique dataset based on the established AirCore passive sampling technique (Karion et al., 2010; Membrive et al., 2017; Engel et al., 2017; Laube et al., 2020; Wagenhäuser et al., 2021; Tans, 2022). In this case, a very large AirCore was flown alongside a cryogenic whole-air sampler, which allows for an independent verification of the AirCore method; something that has not been performed for halogenated species before. A similar verification for the major anthropogenic greenhouse gases CO_2, CH_4, N_2O, and SF_6, along with additional details about the balloon flight can be found in our companion paper, i.e., Schuck et al. (2025). In addition, due to the increased volume of the stratospheric and upper tropospheric air that was retrieved with this AirCore, a much-improved number of halogenated trace species (as compared to the previously published seven in Laube et al., 2020, and Li et al., 2023: SF_6, CFC-11, CFC-12, CFC-113, HCFC-22, H-1211, and H-1301) could be quantified (including CFCs, halons, HCFCs, HFCs, PFCs, and chlorocarbons), alongside retaining a relatively good altitude resolution. Describing the details of the employed methods and evaluating and comparing the results from both instruments are the primary focus of this manuscript.

2 Methods

The results presented below are based on the flight of a gondola weighing approximately 345 kg, which was lifted to $\sim$ 32 km by a large balloon launched by the French Space Agency CNES on 12 August 2021 from the Esrange base near Kiruna, Sweden (67.8883° N, 21.0847° E, 331 m a.s.l.) as part of the EU infrastructure Hemera. Apart from the two instruments described here the payload contained several more, which focused mainly on measurements of major greenhouse gases and for which results are described elsewhere (Schuck et al., 2025).

2.1 Cryosampling

The cryogenic whole-air-sampler has been operated for several decades (largely by the University of Frankfurt, e.g., Schmidt et al., 1987; Engel et al., 2002, 2009) and is one of the most well-established stratospheric air sampling platforms in existence. Its ability to retrieve large air samples from the low-pressure stratosphere has repeatedly proven extremely useful for the investigation of a multitude of trace gases (including, in some cases, their isotopic composition, e.g., Röckmann et al., 2011); especially at altitudes outside of the reach of aircraft (above $\sim$ 20 km), with the cryosamplers able to reach up to $\sim$ 40 km. As it has been described in detail multiple times, we here only present a brief summary of its operating principles: it consists of a Dewar vessel filled with liquid neon and cooling a number of electro-polished stainless-steel containers to around −240 °C. This setup acts as a cryopump when one of the containers is opened by telecommand during the flight, thus allowing the collection of several litres of air over well-defined and narrow altitude ranges. Sampling is concluded by mechanically crushing a gold tube that is part of the inlet and therefore cold-welding the container shut. More details on this particular flight can be found in a companion paper (Schuck et al., 2025). Most importantly, the inlets of five containers were equipped with cotton filters to catalytically prevent the sampling of ozone. These filters are known to remove O_3 from air samples without affecting other trace gases (Hofmann et al., 1992; Persson and Leck, 1994). They were tested prior to the campaign under various conditions and found to perform excellently for CO_2, CH_4, and OCS. A manuscript with more lab test details is in preparation. From the available total of 15 canisters, 13 samples could be successfully collected, four of which had a catalyst. The total weight of the cryosampler excluding the (required) gondola is around 60 kg.

2.2 AirCore technique and MegaAirCore

The AirCore was invented at the NOAA Global Monitoring Labs (Karion et al., 2010) and is a passive sampling devices based on a long (normally up to $\sim$ 100 m, except for the "high-resolution" AirCore: 300 m, see Membrive et al., 2017) coil of extremely thin-walled stainless-steel tubing. Due to the low weight (typically between 2 and 5 kg) these can be launched up to $\sim$ 35 km using comparably low-cost weather balloons. As the tubing is open to outside air on one end, it empties during ascent, and then collects a vertical profile of air after the balloon has burst, i.e., during its descent on a parachute. As the internal diameter of the tubing is typically very small (3–8 mm), diffusion limits mixing inside the AirCore coil (i.e., over the length of the tube), enabling subsequent trace gas analysis and reconstruction of the vertical mixing ratio distributions provided the payload is retrieved and measured within a few hours after landing. An alternative is the prevention of mixing by storing segments of AirCore air in so-called subsamplers (Mrozek et al., 2016; Laube et al., 2020), which is essential for more time-consuming measurements, or in the case of balloons being carried out far away from the analytical equipment after the launches. Typical AirCore volumes are between 500 and 1500 mL (exception again Membrive et al., 2017: $\sim$ 3 L).

The AirCore used in this study is the so-called "MegaAirCore" (MAC); a definitive exaggeration regarding its name, as it is neither in terms of its length (230 m) nor internal volume (11.1 L) a million times larger than a normal-sized AirCore. The MAC weighs around 20 kg and was constructed specifically for this flight. It consists largely of two connected pieces of coiled tubing, i.e., 170 m of 1/4 in. tubing (inner radius: 5.842 mm, stratospheric end) and 60 m of 1/2 in. tubing (inner radius: 11.684 mm, tropospheric end), both of which were stainless steel which had been Silco™-1000-coated to provide extra trace gas inertness. Due to the long

flight duration of ∼ 5.5 h and the cold stratospheric and upper tropospheric temperatures (∼ −72 °C in the vicinity of the tropopause), the MAC was heated with heating foil (heating power: 130 W m^{-2}, 24 V, from Osnatherm GmbH) and using a power bank (capacity: 52 800 mAh, from XTPower.com) to between 10 and 13 °C throughout the entire flight. This temperature was monitored with two Arduino data loggers (from Adafruit Industries, LLC, type: Feather) containing five temperature sensors each, which were attached to the coils in different locations (Fig. 1), notably including in the vicinity of the inlet which is most exposed to the cold surroundings. The purpose of these coil temperature stabilisation and control procedures was to avoid any loss of the target trace gases – some of which have relatively high boiling points of around 90 °C – to the internal AirCore surfaces. All air entering the MAC was dried using a stainless steel cartridge filled with loosely packed $Mg(ClO_4)_2$ as is common for the AirCore technique (Karion et al., 2010; Membrive et al., 2017; Laube et al., 2020). Further temperature stability was provided by placing the coils inside a PE-foam-based package (PLASTAZOTE® low density polyethylene foam LD29, blown with N_2 to prevent any target trace gas contamination) as well as covering the outsides of this parcel with aluminium foil (Fig. 1). The mounting of both the MAC and the cryosampler on the well-established TWIN gondola (Schmidt et al., 1987; Engel et al., 2002) is also shown in Fig. 1.

2.3 Subsampling

As halogenated trace gas analysis was not possible on site, the air collected with the MAC needed to be swiftly divided into sections to prevent further mixing, which was achieved using a subsampling technique (Laube et al., 2020). First, shortly after landing the MAC inlet valve was closed manually by the recovery team to prevent extended exchange of the sampled air with near ground outside air. This is less time-critical for the MAC in comparison to other AirCore devices (Karion et al., 2010; Membrive et al., 2017), as only the stratospheric and upper tropospheric part was being analysed subsequently. The gondola was then transported back to the launch location via helicopter, which caused, when also including the time required for dismounting the MAC from the gondola and preparing it for subsampling, a delay of ∼ 3.5 h; the subsampling procedure itself taking ∼ 1.25 h. These times are important as mixing induced by diffusion within the MAC was possible prior to subsampling, which affects the achievable altitude resolution. Two exemplary estimates of the root mean square molecular diffusion over the entire period for SF_6, and CFC-11 can be found in the Supplement (Fig. S1). These are on the order of 1 m in both cases, equivalent to ∼ 27 mL in the most important 1/4 in. part of the MAC. Overall, it is worth noting that the gases analysed for the MAC have much smaller diffusion coefficients than CO_2 and CH_4 (e.g., Table S1 in Martinerie et al., 2009), which helps limiting such mixing effects. To provide visual comparability, similar molecular diffusion plots for CO_2 and CH_4 have also been included in the Supplement (Fig. S1).

The stratospheric end of the MAC was then connected to a 1/4 in. stainless steel cross (Swagelok™) with a vacuum pump (Edwards nXDS10), a high precision pressure sensor (MKS Baratron, range 0–2000 mbar), and a subsampler at the three other ends (see schematic in Fig. S2). The latter device was almost the same as the Improved Subsampler (ISS) described Sect. S1.1.1 of Laube et al. (2020). It consisted of a central 32-port 1/8-in. valve (from VICI, Switzerland), with a common in- and outlet, as well as loops of 1/4 in. stainless steel (∼ 20 mL volume each) attached to each but the first two pairs of ports. The first pair of ports was blanked for a default position that can be exposed to lab air when connecting the AirCore; whereas the second pair was connected to a larger sample (∼ 103 mL) made from connecting two 50 mL stainless canisters with 90°-angled connectors to form a "loop". This larger sample was installed to collect and store the first bit of air contained in the MAC, which was expected to consist almost entirely of remaining fill gas (here: nearly trace gas-free N_2, details in Sect. 3.1). The other 14 loops were intentionally smaller to enhance the attainable altitude resolution, which is otherwise rather limited as the passive sampling techniques yields increasingly smaller amounts of air at the much-decreased pressure at higher altitudes. Each loop of the subsampler had been leak-checked and conditioned via five fill-evacuate cycles with AirCore fill gas prior to the launch and left filled to ∼ 1 bar. Directly before subsampling each loop was pumped down to < 1 mbar in a first cycle, and to < 0.01 mbar in a second one; with a third cycle to ascertain that the vacuum was holding. Then the MAC was opened with the ISS in position 1 (blanked) and the valve to the pressure sensor open (but closed shortly afterwards) to determine the pressure inside the AirCore, which is typically slightly above ambient due to the gradual warming of the tubing after landing (i.e., in the hangar). The tropospheric end of the AirCore was then opened to avoid pressure gradients between the subsampler loops, followed by the opening of the stratospheric end to each loop successively. The same procedure was repeated for two further subsamplers of the same build (but each having 15 loops at 103 mL), which were also constructed specifically for this flight. Finally, 6 SilcoCans™ (volume: ∼ 400 mL) were filled from the MAC in the same way, resulting in a total subsampled volume of 5.9 L, equivalent to 53 % of the full MAC volume (which is why opening the MAC on the tropospheric side for subsampling did not lead to sample contamination with lab air). Also similar to Laube et al. (2020), all metal subsampler surfaces were Silco-1000-treated to improve surface inertness during sample storage.

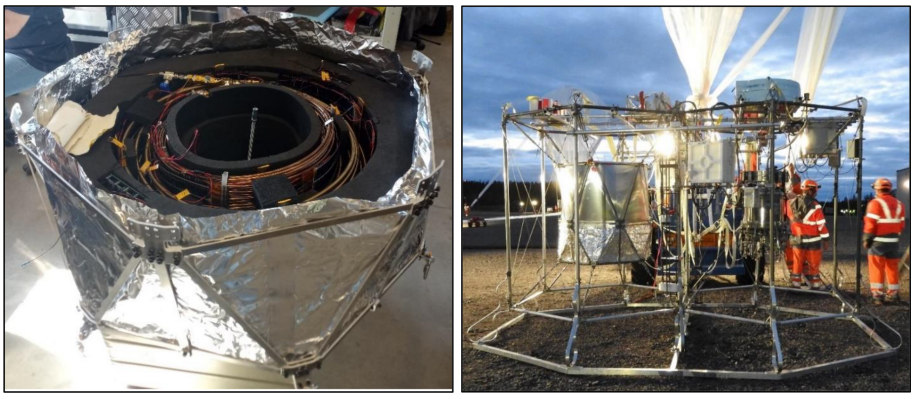

Figure 1. Left: The MegaAirCore (MAC) tubing inside its two layers of insulation. Also visible are several of the temperature sensors deployed to monitor the temperature of the tubing in various places. Right: Gondola just before launch with the MAC parcel mounted low inside the lefthand side hexagon, and the cryosampler inside the righthand side one. Copyright Johannes C. Laube (left) and CNES/Prodigima – Romain Gaboriaud (right).

2.4 Analytical techniques for trace gas analysis and quality assurance

After shipping the samplers back to Germany, dry air mole fractions of halogenated trace gases (referred to here as mixing ratios) were derived using three measurement systems. At Forschungszentrum Jülich (FZJ), all samples (MAC + CRYO) were processed with an analytical system and methodology equivalent to a previously well-established one (Laube et al., 2010, 2020; Leedham Elvidge et al., 2018; Adcock et al., 2021). This newer system has recently been proven to perform equally well (also in comparison to other internationally recognised measurements) for eight CFCs over a temporal range of several decades at mixing ratios between 0.06 and ∼ 80 ppt (Western et al., 2023). Trace gases are being cryogenically extracted and pre-concentrated using an ethanol/dry ice mixture, then thermally desorbed with freshly boiled water, separated by gas chromatography (Agilent 6890 GC with a 60 m long GS GasPro column temperature-programmed to heat from −10 to 200 °C) and detected at high mass resolution (∼ 1000 at 5 % peak height) with a triple-sector mass spectrometer (Waters AutoSpec MS) in selected ion monitoring (SIM) mode. Typical detection limits for the trace gas analysis of a few hundred mL of air are in the lower and sub-ppq (parts per quadrillion) range. The analytical system at Frankfurt University (GUF, CRYO measurements only) is similar in many ways, so we only point out the significant differences here: The cryogenic extraction and pre-concentration is based on a Stirling cooler and trace gas desorption occurs via resistive heating (Schuck et al., 2018). While a very similar GC (Agilent 7890) and the same column (albeit at only half the length) are being used, the temperature program only starts at 50 °C (preventing the analysis of very low-boiling species such as SF_6 or C_2F_6), and the MS is a quadrupole-based one (Agilent 5975C). Typical detection limits are in the sub-ppt range with values around 0.1 ppt for most substances discussed here. Additionally, all cryogenically collected samples were analysed at GUF for their content of SF_6 and CFC-12 with a well-established system based on gas chromatography with electron capture detection (GC-ECD, Jesswein et al., 2021). In total, 39 halogenated species could be successfully quantified, with 24 measured on two analytical systems. More measurement details, including on average precisions, calibration scales, ions used for quantification, and the level of agreement between labs, can be found in Tables S1 and S2 in the Supplement. Additionally, the main working standard (consisting of clean air collected with a trace gas-free metal-bellows compressor in the Taunus mountains near Frankfurt) used for assigning mixing ratios to samples at GUF was transferred to FZJ and measured alongside the cryosampler, thus enabling a consistent calibration scale for all species reported. As a brief summary of this comparison, 50 % of measurements agreed within 1 standard deviation, and 45 % within 2 standard deviations. More details can be found in the Supplement.

3 Results and discussion

3.1 Quantification of the fill gas fraction remaining in the AirCore

One of the main challenges of the AirCore technique is the determination of the exact amount and location of fill gas remaining inside the tubing at the start of the descent part of the balloon flight. This fill gas portion mixes with the uppermost air sampled and therefore complicates the determination of trace gas mole fractions as well as the retrospective altitude assignment procedure. Commonly this is being addressed by using a fill gas with a CO mole fraction (1–10 part per million, ppm) that is much higher than those typically found in the middle stratosphere (10's of part per bil-

lion, ppb). This does however create some uncertainty in the air collected at the highest altitudes, which presents a mixture of the two concentrations that can only be constrained with theoretical calculations. To circumvent this problem – and to also have a fill gas fraction quantifiable with the mass spectrometer system at hand – the fill gas employed here was virtually trace gas-free N_2, with two exceptions. These were (i) small (sub- to low part per trillion, ppt) impurities that could be corrected for, as well as (ii) ~ 160 ppt of perfluoro triethylamine (PFTEA, $C_6F_{15}N$), which is not currently present in the unpolluted atmosphere in detectable amounts (detection limit of the MS system: ~ 0.01 ppt for a 100 mL sample measured at m/z 114, i.e., the $C_2F_4N^+$ fragment). A sample of the undiluted fill gas was measured close in time to the MAC samples to ensure appropriate calibration.

In addition, the sensitivity drift of the analytical system over the course of a measurement day (11–16 h) needs to be corrected for. This is typically done by interspersing a "working standard" of air with well-known and close-to-atmospheric mixing ratios in between sample measurements. However, as the PFTEA is not present in the utilised standard, a substitute trace species needed to be found which showed a reliable response ratio to PFTEA over time, i.e. within one day as well as, ideally, over longer periods of weeks and months. Using nine occasions between 2017 and 2023 where varying amounts of the fill gas (15–100 mL) were measured repeatedly over the course of one day (including at very different times), six compounds were evaluated for this purpose. H-1211 (CF_2BrCl, measured on m/z 129) gave the most consistent ratio between the signal area of PFTEA in the fill gas and the H-1211 peak area in the surrounding standards interpolated to the time of the fill gas measurement (average standard deviation of 1.4 %). As our best estimate of the fill gas content uncertainty, we here use the square root of the sum of squares of (i) the aforementioned uncertainty in the response ratio (except for fill gas signals close to the detection limit, i.e. fill gas fractions less than ~ 0.3 %: independently determined average precision: 4.6 %), and (ii) the precision of the H-1211 measurements on the respective day.

Figure 2 shows the determined fill gas fractions as a function of the subsampled volume including their uncertainties. As can be seen, the fill gas fraction drops rapidly to ~ 0.2 % after ~ 500 mL. After that, values do not consistently decrease further instead showing variability between fill gas fractions of 0.3 % and below detection limit of around 0.05 %. This is likely caused by a small fraction of fill gas remaining in the subsamplers after conditioning (and prior to filling). It does not cause a problem with the correction as the same fill gas was used for both the MAC and the subsamplers prior to filling. To quantify how much fill gas might be originating from the subsamplers, we perform two calculations of the total volume of fill gas left in the MAC: Firstly, via the minimum pressure measured during the balloon flight (11.05 mbar at the highest altitude) and the total AirCore volume and final pressure after landing, which yields 128.6 mL. Secondly, from simply summing up all fill gas volumes determined through the PFTEA measurement-based method, which gives, when corrected for the coil temperature changes from 19 °C during subsampling to on average 11.4 °C during the flight, 132.6 ± 4.5 mL. The two estimates are not significantly different without even considering the radiosonde pressure uncertainty (< 0.1 hPa), with a total of 4.0 ± 4.5 mL or on average 0.07 % of the total remaining fill gas amount possibly contributed by the remaining subsampler filling.

Finally, there is one distinct outlier in Fig. 2 (circled), i.e., the anomalously high 3.75 % of fill gas determined in the last loop of the first subsampler. Due to the cyclic nature of the central subsampler valve, this loop is directly adjacent to the initial position before subsampling, in which the valve remained for ~ 10 min during (i) the pressure measurement of the MAC, and (ii) the equilibration to ambient pressure after opening the tropospheric end valve of the MAC. The likeliest explanation for this outlier is therefore some cross-port leakage during that time, aided by the ~ 1 bar pressure gradient between the evacuated loop and the MAC. All other loops where however only exposed to similar pressure gradients for 20 s as the rest of the subsamplers where filled much faster. This would, when scaling the 3.75 % and the 10 min exposure time, result in a cross-contamination of each sample with ~ 0.1 % of the previous one. Laboratory tests were carried out prior to the campaign, when adjacent loops of this exact subsampler were filled with clean air from the "working tank" (see Sect. 2.3) and trace gas-free synthetic air. This yielded, after storage times of up to 23 d, cross-port contamination effects of 0.2 %–0.5 %. Importantly, increasing storage time had no discernible effect on these numbers and there was also no detectable contamination with lab air. We cannot constrain this cross-contamination estimate further here, but it is worth keeping this effect in mind as something that could slightly bias the determined mole fractions, especially in regions of steep concentration gradients. However, as opposed to the first one, the other two subsamplers were newly built at the time of the campaign and are likely to have performed better due to having experienced less wear and tear on their central valves. It is also important to note that cross-port contamination effects are greatly enhanced by pressure gradients between individual loops. This is something that occurs during the lab tests as evacuation of the inlet line (including the adjacent loop) needs to take place when switching between different filling gases. Such potential issues are however minimised with the applied constant pressure filling method. We conclude that the best estimate of cross-port contamination during the MAC subsampling is ~ 0.1 % or less except for the one outlier discussed above.

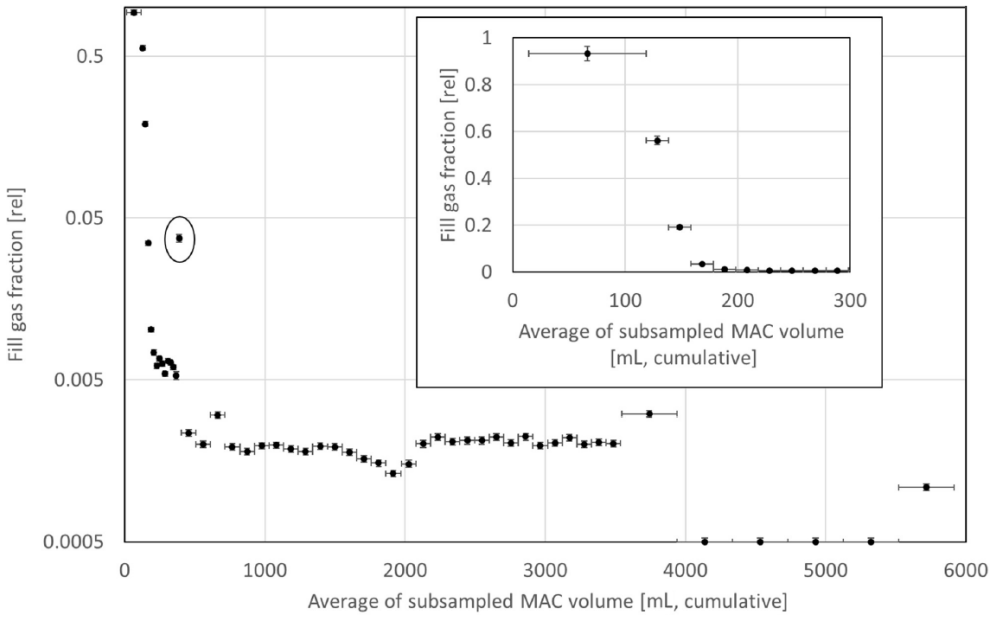

Figure 2. Fill gas fraction contained in the subsamples collected from the MAC as a function of the cumulative subsampled volume (averaged per sample) as determined from the content of PFTEA. The inset illustrates the rapid drop in fill gas fraction over the first 10 samples on a non-logarithmic scale. For four samples the PFTEA signal was too small to be quantified, these are shown as the detection limit (0.0005). Vertical error bars depict the analytically determined fraction uncertainty, whereas horizontal error bars refer to the sample size. The circled data point shows unusually high PFTEA, which is likely caused by the subsampling procedure. Further details can be found in Sect. 3.1.

3.2 Vertical atmospheric distributions of halogenated trace gases

Assigning altitudes to CRYO-based samples is rather straightforward as the times, pressures and GPS altitudes at the time of opening and closing the individual canisters are well known (Schuck et al., 2025). This procedure is more complicated for an AirCore in general as only one sample is being collected over the entire flight. The altitude assignment procedure therefore ideally considers multiple influential factors such as pressure and temperature gradients inside the very long tubing, Taylor and molecular diffusion, or loss of air after landing due to the heating of the AirCore (Karion et al., 2010; Tans, 2022). This is somewhat simplified by the MAC as flown here, as the controlled and relatively slow descent speeds (Fig. 3) prevent pressure gradients, and the active heating of the tubing does not generate any substantial temperature changes (see Sect. 2.2). In addition, the novel fill gas correction method allows for an improved and straightforward calculation of the portion of atmospheric air sampled. Therefore, the MAC altitudes can be derived by calculating the amount of air collected via a simple temperature and pressure correction (through the ideal gas law) of the fill gas-corrected number of moles inside each of the subsampler loops. This is done cumulatively starting with the lowest pressure reached during the flight, following the methodology described in Sect. S1.1.3 of Laube et al. (2020).

3.2.1 SF_6 and CFC-11

Figure 3 shows the vertical profiles of SF_6 and CFC-11, as derived from the MAC and CRYO. CRYO mole fractions of both species were merged from the measurements at GUF and FZJ and, for SF_6 only, primarily published in the companion paper of Schuck et al. (2025). For SF_6, very good agreement with the MAC is observed for 11 of the 13 CRYO samples. Especially notable is that both MAC and CRYO capture the relatively shallow layer of low SF_6 mixing ratios around 24 km that has been observed by CH_4 in situ measurements on the same gondola (Schuck et al., 2025). This is somewhat contrasting our previous estimate of the average molecular diffusion inside the MAC, which actually exceeds the subsample size at these altitudes (Sect. 2.2); although this might qualitatively be reconciled by the fill gas spiking correction being able to remove some of the mixing retrospectively (Sect. 3.1). The latter is especially pronounced at the high-altitude end of the profile where fill gas fractions are highest. Nevertheless, we have also displayed outer error bars in Fig. 3, which represent the altitude range equivalent to root mean square molecular diffusion (see Fig. S1 for more calculation details). It should be noted, though, that these are not actual altitude uncertainties but represent the altitude range over which diffusion has an influence.

The two CRYO samples that for SF_6 do not agree with the MAC within their 1 sigma measurement uncertainties are close to 20 km, i.e., in the profile part with the steepest mix-

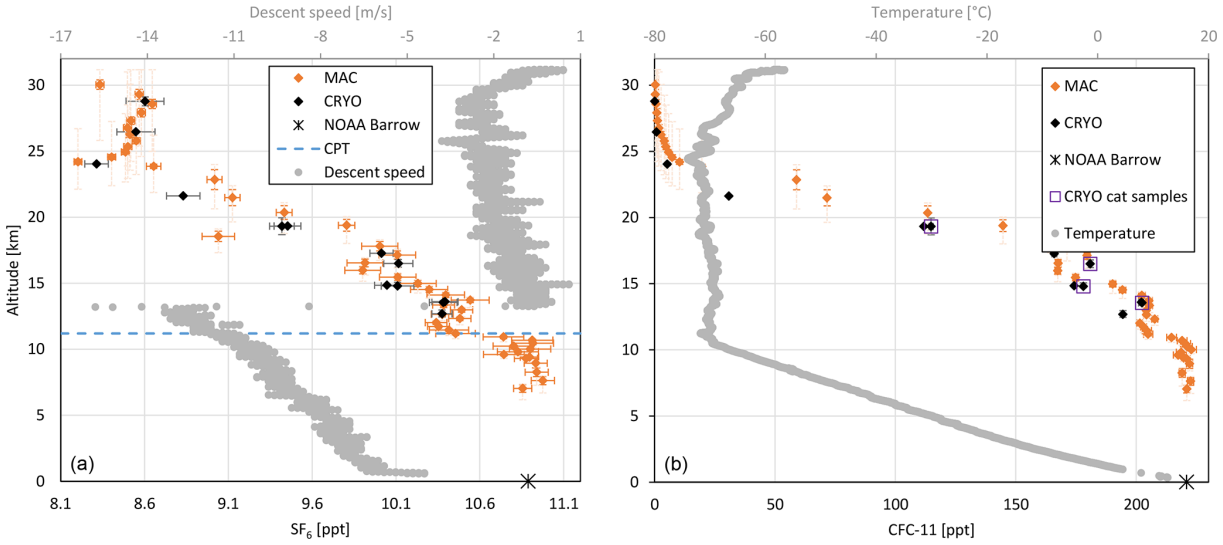

Figure 3. (a) Vertical distribution of SF_6 mixing ratios on 13 August 2021 near Kiruna, Sweden from the middle troposphere to the middle stratosphere as derived for the MegaAirCore (MAC, orange) and the Cryosampler (CRYO, black). Vertical error bars represent the altitude range over which was sampled, whereas, for the MAC only, vertical outer (dashed) error bars represent the altitude range equivalent to root mean square molecular diffusion. Horizontal error bars are equivalent to 1 standard deviation from the measurements (see text for further details). CRYO results are the average of multiple measurements carried out at the University of Frankfurt and Forschungszentrum Jülich. Also shown are (i) the monthly mean mixing ratio of SF_6 from the polar ground-based observatory at Pt. Barrow, Alaska (black star, publicly available data from the NOAA Global Monitoring Labs: https://gml.noaa.gov, last access: 5 January 2025), (ii) the cold-point tropopause (CPT, blue-dashed), and (iii) the descent speed of the gondola carrying the instrument (grey, on secondary x axis). Three MAC samples with fill gas contents of 20 % or more have been excluded due to the additional uncertainties introduced by the fill gas content corrections (see Sect. 3.1). **(b)** The same as panel **(a)**, but for CFC-11, and with (i) four CRYO samples with an O_3-scrubbing catalyst at the inlet highlighted (black circles surrounded by empty purple squares), and (ii) ambient temperature plotted on the secondary x axis (grey).

ing ratio gradient. This discrepancy is likely caused by diffusion leading to mixing inside the MAC, which is known to lead to smoothing effects in AirCore devices (e.g., Membrive et al., 2017). In this case it results in an asymmetric shift in the profile towards higher MAC mole fractions due to the influence of relatively stable mole fractions above ∼ 24 km and further increasing ones below. This is exacerbated here by

i. the relatively large internal diameter of the MAC not limiting diffusion as much as in the much narrower commonly used lower-volume AirCore devices (Tans, 2022),

ii. the long delay between the start of the balloon descent and the subsampling of the MAC (see Sect. 2.2) leading to more molecular diffusion (as indicated by the outer error bars in Fig. 3), and

iii. additional MAC smoothing being caused by the transition from 20 mL to ∼ 100 mL subsamples which occurs at ∼ 24 km, i.e., directly at the upper end of the largest mixing ratio gradient. This is likely the dominant factor here, as otherwise the capturing of the sharp feature of low SF_6 mixing ratios at 24 km cannot be explained.

The MAC-CRYO comparison for CFC-11 supports the mixing effect hypothesis. Due to chemical decay in the stratosphere, the mixing ratio gradient of this CFC with altitude is much more pronounced than for the nearly inert SF_6, which should lead to more diffusion-induced mixing. This is exactly what is being observed, with five of the six CRYO samples collected above 19 km exhibiting significantly lower mixing ratios than those of the MAC; the only exception being one of the two CRYO samples at ∼ 19.3 km, which was collected over a much larger altitude range than the adjacent one. Similar differences were observed for CH_4 when comparing CRYO samples and smaller AirCore devices (Schuck et al., 2025).

Lastly for the MAC only, one sample at ∼ 18.5 km looks anomalously low for SF_6, with no correlated value visible for CFC-11 or almost all other species (except for C_2F_6 and CFC-13, both of which elute close in time to SF_6 during GC-MS analysis). While we cannot fully rule out that there was a temporary measurement system glitch, we have kept these values in the dataset as no obvious (physical) reason for excluding this sample has been found.

In addition, altitude-related discrepancies are observed when just looking at CRYO samples: of the three sample pairs collected at similar altitudes, agreement within even two standard deviations (instead of the one standard deviation in Fig. 3) is observed for only one in the case of CFC-11. However, for SF_6 all three sample pairs agree within

two standard deviations. This reflects a wider tendency as better agreement is found for longer-lived species such as CFC-115, HFC-23, or c-C_4F_8, which have less steep mole fraction gradients. Therefore, these differences are likely strongly influenced by the slightly different altitude ranges over which sample pairs were collected, in combination with pronounced mole fraction gradients in their immediate vicinity as well as, potentially, atmospheric variability.

Also visible in Fig. 3 is that the cut-off of the balloon with a much faster descent on a parachute from ~ 13.3 km downwards has no apparent influence on the derived MAC mole fractions; whereas the cold-point tropopause (CPT) at ~ 11.2 km can be clearly identified as a transport barrier due to the disconnect between SF_6 and CFC-11 concentrations above and below. Further down, it is reassuring to see that the middle tropospheric MAC data for both gases agree very well with the ground-based mole fractions from a similar latitude, i.e., the observatory at Pt. Barrow, Alaska, USA (71.3° N, 156.6° W, part of the NOAA Global Monitoring Labs global network). Notable is also the region between the tropopause and about 14 km, which shows a less pronounced gradient in trace gas mole fraction than further up. This is likely a region influenced by enhanced troposphere-stratosphere exchange, which is often found in the extra-tropical tropopause region in late summer and autumn (e.g., Hauck et al., 2020). Such a hypothesis is supported by the observed discrepancy between the CPT at 11.2 km and the WMO-defined tropopause at 10.5 km (Schuck et al., 2025), which indicates a weakened tropopause transport barrier.

3.2.2 Problematic species

The laboratory storage tests mentioned in Sect. 3.1 were also used to determine the long-term stability of the target species prior to the campaign. No significant effects were found for most species after up to 23 d, although the spread of the results from the individual subsampler loops was rather high at around 5 %. This is likely related to some shortcomings of the testing method, with the uncertainties introduced by the fill-evacuate cycles as well as the slight differences in fill pressure in each loop; none of which occur during MAC/AirCore subsampling. While this could mean that potentially all mole fractions might be biased by up to 5 % this is highly unlikely due to

i. the much more compact correlations observed in the MAC profile,

ii. the much-improved volume/internal surface area ratio in the larger subsamplers, and

iii. the low mixing ratios observed for many gases near the top of the profile, which are often close to the detection limit (see, e.g., CFC-11 in Fig. 3) and therefore evidencing the leak-tightness of the subsampling system.

Storage stability exceptions were found only for some of the shorter-lived species (CH_2Cl_2: 1 out of 3 loops +15 % only in the case of maximum storage time, i.e., after 23 d; $CHCl_3$: 2/3 loops at +10 % and +16 % after 23 d only; CH_3Cl: mixing ratios in all loops consistently increasing with increasing storage time after more than 10 d by up to 30 % – consequently not measured in MAC) as well as HFC-23. The latter is a well-known problem as small amounts of this gas are emitted by the rotor material (Valcon E®) in the central valve of the subsamplers.

Accordingly, many trace gases show good comparability between CRYO and MAC (see H-1211 in Fig. 4), but for some there are issues with, e.g., contaminations (see Table S1). Figure 4 demonstrates this for CFC-12, for which the middle two MAC subsamplers are randomly contaminated leading to a break-down of its compact correlations with altitude and other trace gases in the middle of the profile. The exact source of this contamination, which also affects c-C_4F_8, HFC-32, HFC-134a, and HFC-227ea, could not be determined subsequently. It should however be noted that (i) both subsamplers were newly built for this flight and might have been insufficiently conditioned (i.e., flushed and heated) beforehand, and (ii) this cannot be a contamination with outside air since there were no leaks found, and other substances were not affected at all. All data from those two subsamplers were excluded for a given trace gas if clear contaminations (defined as variability outside three standard deviation measurement uncertainties) were observed for more than two samples. On the more positive side, the usable part of the data for HFC-32, HFC-143a, HFC-152a, HFC-236fa, and HFC-245fa are to our knowledge a unique in situ-based quantification of the stratospheric distribution of these species (disclaimer: only CRYO GUF measurements available for the latter three of these HFCs).

Also shown in Fig. 4c and d are two HCFCs, i.e., HCFC-22 and HCFC-133a. Here – as well as for the other two HCFCs quantified (HCFC-141b and HCFC-142b) – larger differences are observed between MAC and CRYO samples. However, much better agreement is found for the four CRYO samples with the O_3 scrubbing catalyst in the inlet (highlighted in Fig. 4). In the upper part of the profile, where O_3 mole fractions (on secondary x axis in Fig. 4, derived from a concurrent ozone sonde launch) are still increasing, CRYO and MAC HCFC mole fractions converge again. While we cannot explain this convergence, this is overall a strong indication that the O_3 present in the CRYO samples might affect some species chemically during the sampling or storage process. Note that the main difference in sampling technique between the MAC and the CRYO is that the latter condenses the air and the trace gases which might allow for chemical processes that are otherwise not significant. Two further bits of evidence support this chemical decay hypothesis: firstly, the vertical profiles derived from the MAC are very compact and follow the shape observed for other (more chemically inert) species such as SF_6 much more closely. Even the low mole

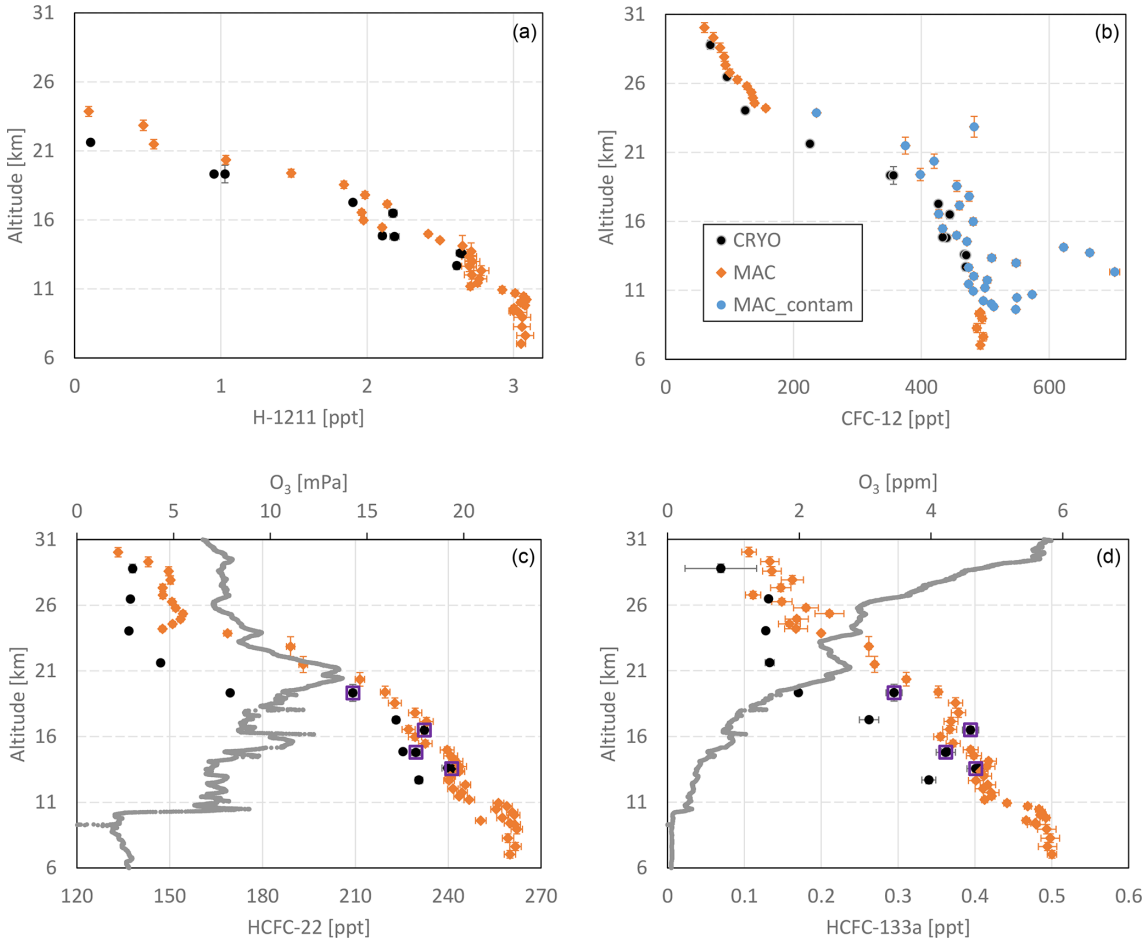

Figure 4. The same as in Fig. 3 but for H-1211 **(a)**, CFC-12 **(b)**, HCFC-22 **(c)**, and HCFC-133a **(d)**, again with four CRYO samples with an O_3-scrubbing catalyst at the inlet highlighted (empty purple squares), and with O_3 partial pressures and mixing ratios on secondary x axes **(c, d)**.

fraction feature near 24 km is present in the MAC profile, but not for the CRYO. And secondly, the recent study of Kolonjari et al., (2024) compared stratospheric HCFC-22 CRYO data with those from a balloon-born remote-sensing instrument, two satellite instruments, and a model. They found that the CRYO samples often exhibited lower mole fractions (up to $\sim$30 %), and this was especially pronounced in the upper part of their comparison altitude range (i.e., between 20 and 25 km). Nevertheless, we have no definitive proof that the CRYO samples are low-biased, nor do we have proof that the MAC samples are completely unbiased; although there are some strong pointers here, and more to follow in the next section.

3.2.3 Potential influence of air masses from the Asian Summer Monsoon

Figure 5 shows the vertical distributions of mole fractions for four species: CCl_4, CFC-113a, CH_2Cl_2, and $CHCl_3$. All of them are displaying a layer of increased MAC-based mole fractions between 9.4 and 10.9 km (potential temperature range: 300 to 305 K), i.e., just underneath the cold-point tropopause at 11.2 km. The mole fractions of CH_2Cl_2, and $CHCl_3$ show particularly high increases. Both gases are known to have increased in concentration in recent years with East Asia being a major driver of the emission increases (Fang et al., 2019; Claxton et al., 2020). Similarly, the Asian Summer Monsoon has been demonstrated as an effective transport mechanism for such emissions into the Upper Troposphere/Lower Stratosphere (UTLS) region, especially in the northern hemisphere (Vogel et al., 2019; Adcock et al., 2021; Lauther et al., 2022; Pan et al., 2024). Similarly, CCl_4 and CFC-113a are also known to have strong sources in the East Asian region (Adcock et al., 2018; Park et al., 2021). Following the methodology of a recent study by Graßl et al. (2024) (who demonstrated the impact of the Asian summer monsoon on the Arctic aerosol budget in summer 2021), we investigated whether artificial surface origin tracers released globally within the Chemical Lagrangian Model of the Stratosphere (CLaMS; e.g., Vogel et al., 2016)

might be associated with the South Asian source region. The latter is defined here as in Graßl et al. (2024) and encompasses the monsoon region including India, Nepal, southern and eastern China, the Bay of Bengal and the Arabian Sea. Indeed, the model data shows some influence of this air (fractions from 1.5 % to 3.5 %) in the vicinity of the launch site (Figs. S3–S5), although it appears to be at slightly higher altitudes (i.e., around 310 K). Note that the CLaMS output in this case is always at 12:00 UTC, whereas the balloon flight took place during nighttime – and that the distribution of the tracer can change significantly within a few hours, especially in the UTLS. Past studies have used more sophisticated techniques to trace the air mass origins (e.g., Adcock et al., 2021). This is however beyond the scope of this technique-focused study. The observed mole fraction enhancement is relatively modest ($\sim$ 15 ppt for CH_2Cl_2, in comparison to several hundred ppt observed at these altitudes above East Asia). It is therefore plausible that the observed feature is indeed influenced by outflow from the Asian Summer Monsoon, which is also known to influence the extra-tropical northern hemispheric UTLS the most in late summer and early autumn (e.g., Ploeger et al., 2015; Lauther et al., 2022).

Moreover, as the attentive reader has probably noticed in Fig. 5, CRYO and MAC sample mole fractions are more scattered and do not agree very well with each other for CH_2Cl_2 and $CHCl_3$. Some of the enhanced MAC mole fractions coincide with samples contaminated with CFC-12 (see Sect. 3.2.2) but others do not. There might therefore be influence from the contamination of the middle two subsamplers here, especially recognisable for CH_2Cl_2, which exhibits a much more compact correlation shape towards the top and bottom of the profile. However, the comparability of CRYO and MAC samples is not very good for most samples, and even catalyst-equipped ones appear not to perform consistently. As the internal surfaces of the CRYO canisters have no inert treatment, and long-term stability issues for more reactive compounds have been previously reported (Laube et al., 2008; Schuck et al., 2020), it is more likely that the uncontaminated MAC samples are the more realistic option here. Nevertheless, in the absence of further extensive stability testing under realistic stratospheric conditions (including O_3), we recommend a cautious approach to the part of the data that consists of short-lived halogenated species.

3.2.4 Derivation of the mean age of air from multiple tracers

Data for three inert gases from the MAC (SF_6, C_2F_6, and HFC-125) and three further ones from the CRYO (HFC-23, C_3F_8, and c-C_4F_8) is of sufficient quality to attempt the determination of the mean age of air (i.e., average stratospheric transit times, a key indicator for the overturning circulation strength). All these gases are principally suitable as age tracers as they fulfil the crucial criteria of chemical inertness as well as monotonically increasing mole fractions in the troposphere over at least a decade (see WMO, 2022 for recent trends and stratospheric lifetimes). For SF_6, the inertness criterion has been found to be not entirely true (Andrews et al., 2001; Ray et al., 2017; Leedham Elvidge et al., 2018), but we here employ a method based on a recent study which allows for the correction of the related effects (Garny et al., 2024a). Also notable is that opposed to the other five gases, which have been known to be suitable for determining mean ages for some time (e.g., Volk et al., 1997; Andrews et al., 2001; Ray et al., 2017; Leedham Elvidge et al., 2018), c-C_4F_8 has only recently been introduced for this purpose by Umezawa et al. (2024). As for the method to derive the mean ages, we here employ a new consolidated reference method for parameterisation of the age spectrum Garny et al. (2024b); corresponding software in Wagenhäuser et al. (2024). This robust and state-of-the-art method includes a good representation of (a) the long tail of the age spectrum as well as (b) the squared width of the age spectrum with mean age. The tropospheric long-term trends utilised are updated ones from Leedham Elvidge et al. (2018) for all gases except SF_6 (Ray et al., 2024) and c-C_4F_8 (Droste et al., 2020).

Figure 6 shows the mean ages as derived from all six gases. Note that the SF_6-based CRYO results are slightly different to those reported in our companion paper (Schuck et al., 2025) as we apply a consistent mole fraction retrieval and uncertainty derivation method for both the FZJ and the GUF dataset. The related differences are well within those uncertainties though. As expected from the mixing ratio profile differences, the discrepancies between MAC and CRYO are on average greatest in the region with the steepest age gradient, i.e., between 19 and 24 km. Otherwise the CRYO- and MAC-based mean ages generally agree well, though the uncertainty ranges sometimes do not overlap. It should be noted, though, that the related error bars in Fig. 6 only represent the measurement uncertainty of the stratospheric samples (1 standard deviation). Considering the uncertainties in the age spectrum parameterisation as well as in the tropospheric trend could add up to 1 month and up to about a year, respectively (Leedham Elvidge et al., 2018; Umezawa et al., 2024). These are not included here to improve the clarity of Fig. 6. However, when adding (a) a 1-month age spectrum parameterisation uncertainty, and (b) the tropospheric trend uncertainties from Leedham Elvidge et al. (2018) for C_2F_6 and HFC-125, and the more recent ones from Umezawa et al. (2024) for all other gases, all but three mean age estimates agree with those based on SF_6 (excluding non-physical negative mean ages near or below the tropopause). Two of these are outliers observed for HFC-125 (Fig. 6). Both can be found in the uppermost subsampler and are most likely to be due to small contaminations, which in the case of age tracers are sufficient to induce a substantial low bias to the derived mean ages.

Also apparent from Fig. 6 is that the mean ages derived from C_2F_6 in the uppermost MAC subsampler are much more scattered. This is likely due to the much smaller sample sizes (less than 1/5th) as compared to the samples below,

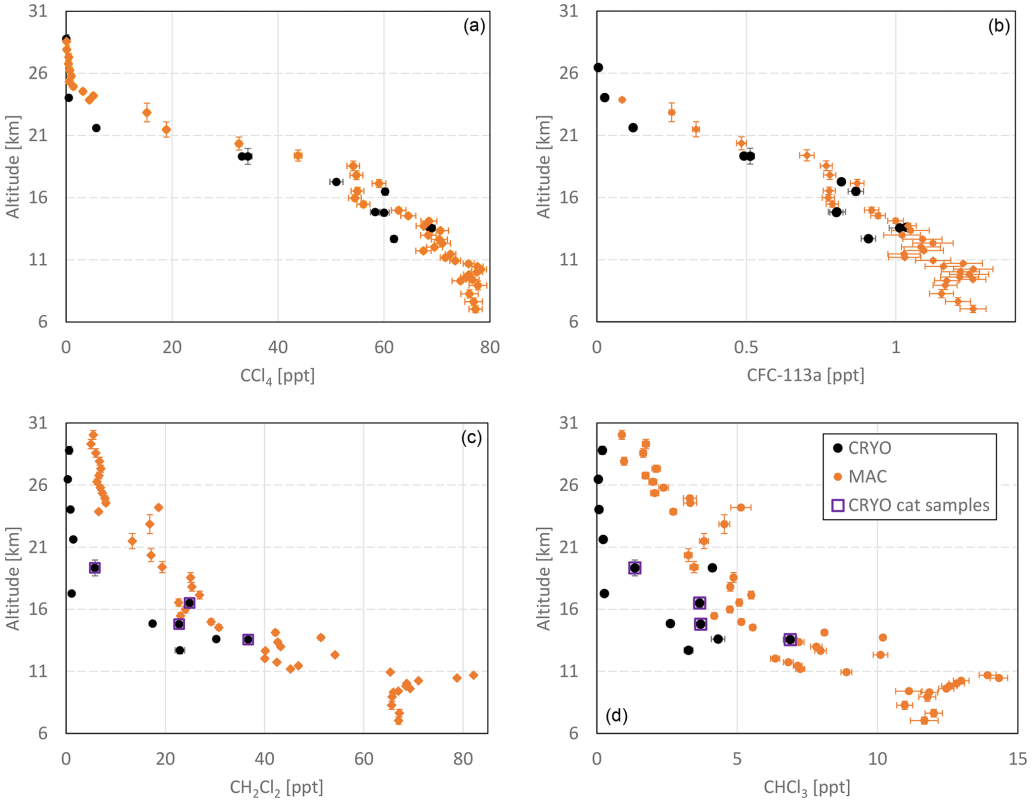

Figure 5. The same as in Fig. 3 but for CCl_4 **(a)**, CFC-113a **(b)**, CH_2Cl_2 **(c)**, and $CHCl_3$ **(d)**.

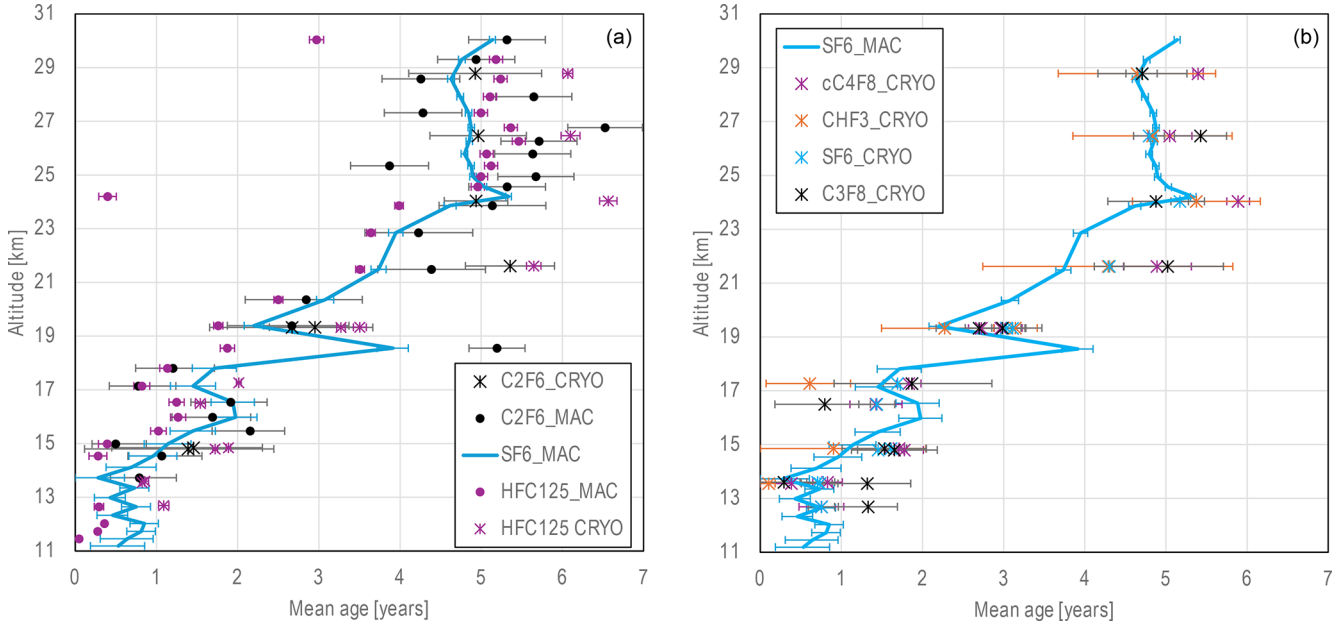

Figure 6. **(a)** Mean ages of air versus altitude as derived from tropospheric trends and stratospheric mole fraction as available from the MAC and the CRYO samplers for C_2F_6, SF_6 (MAC only), and HFC-125. **(b)** The same but for C_3F_8, SF_6 (including CRYO), c-C_4F_8, and CHF_3. All SF_6-based ages have been sink-corrected according to Garny et al. (2024a).

which limits the signal size for C_2F_6. The relevant error bars in Fig. 6 therefore are likely an underestimate of the actual uncertainty, highlighting the statistical limitations associated with very small sample sizes that do not allow for repeat measurements. As for the CRYO-based estimates, the mean ages derived from C_3F_8 and c-C_4F_8 compare well with those from the other tracers and have much smaller error bars than those reported in Umezawa et al. (2024). This is entirely due to the better stratospheric measurement precisions ($\sim 1\%$ as compared to $\sim 6\,\%$, see Table S1) in this work, and underlines the principal suitability of these two species as age tracers.

4 Conclusions

In this study we analysed subsampled air from a very large AirCore for its content of 30 halogenated trace gases and demonstrated the useability of 26 of those (Table S1). As the dataset shows, close attention needs to be paid to the leak-tightness of the entire AirCore and subsampling system as well as thorough flushing to prevent as many contaminations as possible. A new method to correct for the remaining fill gas in the MAC by spiking it with a gas (a) measurable with mass spectrometry alongside the target gases, and (b) currently not present in the atmosphere, was employed successfully. In addition, the CRYO enabled access to even more trace species due to the larger sample size but was also found to exhibit previously unreported problems with some species (HCFCs) that were thought to be stable in this sampler. Here, the catalytic destruction of O_3 in the sample canister inlet led to a much better agreement with the MAC-based samples, pointing towards chemical decay of some species during cryosampling and/or storage. Overall, the quality of the MAC data is good for a maiden flight, with several of the more inert species yielding sensible and CRYO-comparable results when deriving mean ages.

Generally, the MegaAirCore (MAC) profiles successfully demonstrate the advantages of a large AirCore compared to a cryogenic whole-air sampler (CRYO): 48 instead of 13 viable air samples could be obtained, revealing multiple layering structures in various parts of the stratosphere (similar to the ones observed by the collocated in situ CH_4 instrument in Schuck et al., 2025). This indicates a particularly high vertical stability, which is probably at least in part due to the generally limited vertical mixing/exchange processes in the middle stratosphere that lead to the long transport timescales of the residual overturning circulation. In addition, the MAC enables access to multiple samples deep inside the troposphere, thus allowing for an easier comparison to ground-based measurements. This is something that is not always achievable with the CRYO as due to the limited number of samples the collection is often focused on the harder-to-access higher altitudes. However, cryogenically collected samples allow for larger volumes and are more suitable for collecting air samples over very narrow and well-defined altitude ranges. This could be improved for the AirCore technique by better limiting internal mixing (which can also introduce biases in the vertical distribution, especially in the vicinity of strong concentration gradients), e.g., through further minimising the delay between landing and subsampling – although the feasibility here is very much dependent on the accessibility of the terrain in the landing area. Smaller AirCore devices generally offer easier and therefore faster recoveries, albeit at the cost of less air being available for trace gas analysis. Similarly, lowering the size of the subsamples taken from an AirCore can help to better capture smaller features and/or strong gradients in the vertical mole fraction distributions (e.g., Li et al., 2023) as is demonstrated in the upper part of the MAC profile.

Importantly, this is not a full verification of the AirCore sampling technique as the large balloon utilised here descended much slower for much of the flight. Pressure non-equilibrium effects from the near-freefall at high altitudes during common AirCore flights remain unverified in situ, as do the additional temperature-induced changes in the very cold stratosphere when flying an unheated AirCore. Overall, this dataset adds substantially to the rather sparse in situ-based mean age record (Garny et al., 2024b), and could in the future be, e.g., useful for (a) validating satellite products (Saunders et al., 2025), and (b) deriving constraints on the shape of age spectra with new approaches (Voet et al., 2025; Ray et al., 2024) through the diversity of trace gases that are available.

Data availability. Observational data, including mixing ratios, uncertainties, and mean ages of air, has been made available in a public domain repository at https://doi.org/10.5281/zenodo.15437807 (Laube, 2025).

Supplement. The supplement related to this article is available online at https://doi.org/10.5194/amt-18-4087-2025-supplement.

Author contributions. JCL, TJS, SB, HC, SvH, TK, MEP, TW, AZ, and AE contributed to campaign preparation (including laboratory work on the design and testing of the O_3 scrubbers) and the operation of the instrumentation in the field. TJS and JCL performed post-flight sample analysis. MG, ET, and FV contributed to data analysis and interpretation, whereas BV provided CLaMS model output. JCL drafted the manuscript, and all coauthors contributed to improving it.

Competing interests. At least one of the (co-)authors is a member of the editorial board of *Atmospheric Measurement Techniques* . The peer-review process was guided by an independent editor, and the authors also have no other competing interests to declare.

Special issue statement. This article is part of the special issue "The tropopause region in a changing atmosphere (TPChange) (ACP/AMT/GMD/WCD inter-journal SI)". It is not associated with a conference.

Acknowledgements. We are extremely grateful for the support from the technical staff before, during, and after the campaign, especially from Anne Richter, Andreas Sitnikov, Jochen Barthel, and Vicheith Tan (FZJ), Laurin Merkel (GUF), and Carina van der Veen (Utrecht). Also invaluable was the support from teams at ESRANGE base, from CNES as flight operator and provider of additional ozone sonde data, and from Mélanie Ghysels, Georges Durry, and Nadir Amarouche (provision of ambient pressure data). We acknowledge the work of the NOAA Global Monitoring Laboratory for providing surface measurements of multiple gases for comparison with our data, as well as for the derivation of age of air in the case of SF_6. Last but not least, we very much appreciate the contributions from all anonymous reviewers, which have helped to improve this manuscript considerably.

Financial support. This research has been supported by the European Research Council, EU H2020 (grant nos. 678904 (EXC3ITE) and 742798 (COS-OCS; to Maarten C. Krol)), the EU INFRAIA grant 730790-HEMERA, and the Deutsche Forschungsgemeinschaft (program "The Tropopause Region in a Changing Atmosphere" (TRR 301 – Project-ID 428312742)).

The article processing charges for this open-access publication were covered by the Forschungszentrum Jülich.

Review statement. This paper was edited by Thomas F. Hanisco and reviewed by three anonymous referees.

References

Adcock, K. E., Reeves, C. E., Gooch, L. J., Leedham Elvidge, E. C., Ashfold, M. J., Brenninkmeijer, C. A. M., Chou, C., Fraser, P. J., Langenfelds, R. L., Mohd Hanif, N., O'Doherty, S., Oram, D. E., Ou-Yang, C.-F., Phang, S. M., Samah, A. A., Röckmann, T., Sturges, W. T., and Laube, J. C.: Continued increase of CFC-113a (CCl_3CF_3) mixing ratios in the global atmosphere: emissions, occurrence and potential sources, Atmos. Chem. Phys., 18, 4737–4751, https://doi.org/10.5194/acp-18-4737-2018, 2018.

Adcock, K. E., Fraser, P. J., Hall, B. D., Langenfelds, R. L., Lee, G., Montzka, S. A., Oram, D. E., Röckmann, T., Stroh, F., Sturges, W. T., Vogel, B., and Laube, J. C.: Aircraft-Based Observations of Ozone-Depleting Substances in the Upper Troposphere and Lower Stratosphere in and Above the Asian Summer Monsoon, J. Geophys. Res., 126, e2020JD033137, https://doi.org/10.1029/2020JD033137, 2021.

Andrews, A. E., Boering, K. A., Daube, B. C.,Wofsy, S. C., Loewenstein, M., Jost, H., Podolske, J. R.,Webster, C. R., Herman, R. L., Scott, D. C., Flesch, G. J., Moyer, E. J., Elkins, J. W., Dutton, G. S., Hurst, D. F., Moore, F. L., Ray, E. A., Romashkin, P. A., and Strahan, S. E.: Mean ages of stratospheric air derived from in situ observations of CO_2, CH_4, and N_2O, J. Geophys. Res.-Atmos., 106, 32295–32314, https://doi.org/10.1029/2001JD000465, 2001.

Claxton, T., Hossaini, R., Wilson, C., Montzka, S. A., Chipperfield, M. P., Wild, O., Bednarz, E. M., Carpenter, L. J., Andrews, S. J., Hackenberg, S. C., Mühle, J., Oram, D., Park, S., Park, M., Atlas, E., Navarro, M., Schauffler, S., Sherry, D., Vollmer, M., Schuck, T., Engel, A., Krummel, P. B., Maione, M., Arduini, J., Saito, T., Yokouchi, Y., O'Doherty, S., Young, D., and Lunder, C.: A synthesis inversion to constrain global emissions of two very short lived chlorocarbons: dichloromethane, and perchloroethylene, J. Geophys. Res.-Atmos., 125, e2019JD031818, https://doi.org/10.1029/2019JD031818, 2020.

Dodangodage, R., Bernath, P. F., Boone, C.D., Crouse, J., and Harrison, J. J.: The first remote-sensing measurements of HFC-32 in the Earth's atmosphere by the Atmospheric Chemistry Experiment Fourier Transform Spectrometer (ACE-FTS), Journal of Quantitative Spectroscopy and Radiative Transfer, Volume 272, 107804, https://doi.org/10.1016/j.jqsrt.2021.107804, 2021.

Droste, E. S., Adcock, K. E., Ashfold, M. J., Chou, C., Fleming, Z., Fraser, P. J., Gooch, L. J., Hind, A. J., Langenfelds, R. L., Leedham Elvidge, E. C., Mohd Hanif, N., O'Doherty, S., Oram, D. E., Ou-Yang, C.-F., Panagi, M., Reeves, C. E., Sturges, W. T., and Laube, J. C.: Trends and emissions of six perfluorocarbons in the Northern Hemisphere and Southern Hemisphere, Atmos. Chem. Phys., 20, 4787–4807, https://doi.org/10.5194/acp-20-4787-2020, 2020.

Engel, A., Strunk, M., Müller, M., Haase, H., Poss, C., Levin, I., and Schmidt, U.: Temporal development of total chlorine in the high-latitude stratosphere based on reference distributions of mean age derived from CO_2 and SF_6, J. Geophys. Res., 107, 4136, https://doi.org/10.1029/2001JD000584, 2002.

Engel, A., Möbius, T., Bönisch, H., Schmidt, U., Heinz, R., Levin, I., Atlas, E., Aoki, S., Nakazawa, T., Sugawara, S., Moore, F., Hurst, D., Elkins, J., Schauffler, S., Andrews, A., and Boering, K.: Age of stratospheric air unchanged within uncertainties over the past 30 years, Nat. Geosci., 2, 28–31, 2009.

Engel, A., Bönisch, H., Ullrich, M., Sitals, R., Membrive, O., Danis, F., and Crevoisier, C.: Mean age of stratospheric air derived from AirCore observations, Atmos. Chem. Phys., 17, 6825–6838, https://doi.org/10.5194/acp-17-6825-2017, 2017.

Fang, X., Park, S., Saito, T., Tunnicliffe, R., Ganesan, A. L., Rigby, M., Li, S., Yokouchi, Y., Fraser, P. J., Harth, C. M., Krummel, P. B., Mühle, J., O'Doherty, S., Salameh, P. K., Simmonds, P. G., Weiss, R. F., Young, D., Lunt, M. F., Manning, A. J., Gressent, A., and Prinn, R. G.: Rapid increase in ozone-depleting chloroform emissions from China, Nat. Geosci., 12, 89–93, https://doi.org/10.1038/s41561-018-0278-2, 2019.

Garny, H., Eichinger, R., Laube, J. C., Ray, E. A., Stiller, G. P., Bönisch, H., Saunders, L., and Linz, M.: Correction of stratospheric age of air (AoA) derived from sulfur hexafluoride (SF_6) for the effect of chemical sinks, Atmos. Chem. Phys., 24, 4193—4215, https://doi.org/10.5194/acp-24-4193-2024, 2024a.

Garny, H., Ploeger, F., Abalos, M., Bönisch, H., Castillo, A., von Clarmann, T., Diallo, M., Engel, A., Laube, J. C., Linz, M., Neu, J., Podglajen, A., Ray, E., Rivoire, L., Saunders, L. N., Stiller, G., Voet, F., Wagenhäuser, T., and Walker, K. A.: Age of stratospheric air: Progress on processes, observations and long-term trends, Rev. Geophys., 62, e2023RG000832, https://doi.org/10.1029/2023RG000832, 2024b.

Graßl, S., Ritter, C., Tritscher, I., and Vogel, B.: Does the Asian summer monsoon play a role in the stratospheric aerosol budget of the Arctic?, Atmos. Chem. Phys., 24, 7535—7557, https://doi.org/10.5194/acp-24-7535-2024, 2024.

Harrison, J. J., Boone, C. D., Brown, A. T., Allen, N. D., Toon, G. C., and Bernath, P. F.: First remote sensing observations of trifluoromethane (HFC-23) in the upper troposphere and lower stratosphere, J. Geophys. Res.-Atmos., 117, D05308, https://doi.org/10.1029/2011JD016423, 2012.

Hauck, M., Bönisch, H., Hoor, P., Keber, T., Ploeger, F., Schuck, T. J., and Engel, A.: A convolution of observational and model data to estimate age of air spectra in the northern hemispheric lower stratosphere, Atmos. Chem. Phys., 20, 8763–8785, https://doi.org/10.5194/acp-20-8763-2020, 2020.

Hofmann, U., Hofmann, R., and Kesselmeier, J.: Cryogenic trapping of reduced sulfur compounds using a nafion drier and cotton wadding as an oxidant scavenger, Atmos. Environ. A-Gen., 26, 2445–2449, https://doi.org/10.1016/0960-1686(92)90374-T, 1992.

Jesswein, M., Bozem, H., Lachnitt, H.-C., Hoor, P., Wagenhäuser, T., Keber, T., Schuck, T., and Engel, A.: Comparison of inorganic chlorine in the Antarctic and Arctic lowermost stratosphere by separate late winter aircraft measurements, Atmos. Chem. Phys., 21, 17225–17241, https://doi.org/10.5194/acp-21-17225-2021, 2021.

Karion, A., Sweeney, C., Tans, P., and Newberger, T.: AirCore: An Innovative Atmospheric Sampling System, J. Atmos. Ocean. Tech., 27, 1839–1853, https://doi.org/10.1175/2010JTECHA1448.1, 2010.

Kolonjari, F., Sheese, P. E., Walker, K. A., Boone, C. D., Plummer, D. A., Engel, A., Montzka, S. A., Oram, D. E., Schuck, T., Stiller, G. P., and Toon, G. C.: Validation of Atmospheric Chemistry Experiment Fourier Transform Spectrometer (ACE-FTS) chlorodifluoromethane (HCFC-22) in the upper troposphere and lower stratosphere, Atmos. Meas. Tech., 17, 2429–2449, https://doi.org/10.5194/amt-17-2429-2024, 2024.

Laube, J.: Vertical distribution of halogenated trace gases in the summer Arctic stratosphere based on two independent air sampling methods, Version v1, Zenodo [data set], https://doi.org/10.5281/zenodo.15437807, 2025.

Laube, J. C., Engel, A., Bönisch, H., Möbius, T., Worton, D. R., Sturges, W. T., Grunow, K., and Schmidt, U.: Contribution of very short-lived organic substances to stratospheric chlorine and bromine in the tropics – a case study, Atmos. Chem. Phys., 8, 7325—7334, https://doi.org/10.5194/acp-8-7325-2008, 2008.

Laube, J. C., Martinerie, P., Witrant, E., Blunier, T., Schwander, J., Brenninkmeijer, C. A. M., Schuck, T. J., Bolder, M., Röckmann, T., van der Veen, C., Bönisch, H., Engel, A., Mills, G. P., Newland, M. J., Oram, D. E., Reeves, C. E., and Sturges, W. T.: Accelerating growth of HFC-227ea (1,1,1,2,3,3,3-heptafluoropropane) in the atmosphere, Atmos. Chem. Phys., 10, 5903–5910, https://doi.org/10.5194/acp-10-5903-2010, 2010.

Laube, J. C., Leedham Elvidge, E. C., Adcock, K. E., Baier, B., Brenninkmeijer, C. A. M., Chen, H., Droste, E. S., Grooß, J.-U., Heikkinen, P., Hind, A. J., Kivi, R., Lojko, A., Montzka, S. A., Oram, D. E., Randall, S., Röckmann, T., Sturges, W. T., Sweeney, C., Thomas, M., Tuffnell, E., and Ploeger, F.: Investigating stratospheric changes between 2009 and 2018 with halogenated trace gas data from aircraft, AirCores, and a global model focusing on CFC-11, Atmos. Chem. Phys., 20, 9771–9782, https://doi.org/10.5194/acp-20-9771-2020, 2020.

Lauther, V., Vogel, B., Wintel, J., Rau, A., Hoor, P., Bense, V., Müller, R., and Volk, C. M.: In situ observations of CH_2Cl_2 and $CHCl_3$ show efficient transport pathways for very short-lived species into the lower stratosphere via the Asian and the North American summer monsoon, Atmos. Chem. Phys., 22, 2049–2077, https://doi.org/10.5194/acp-22-2049-2022, 2022.

Leedham Elvidge, E. C., Bönisch, H., Brenninkmeijer, C. A. M., Engel, A., Fraser, P. J., Gallacher, E., Langenfelds, R., Mühle, J., Oram, D. E., Ray, E. A., Ridley, A. R., Röckmann, T., Sturges, W. T., Weiss, R. F., and Laube, J. C.: Evaluation of stratospheric age of air from CF_4, C_2F_6, C_3F_8, CHF_3, HFC-125, HFC-227ea and SF_6; implications for the calculations of halocarbon lifetimes, fractional release factors and ozone depletion potentials, Atmos. Chem. Phys., 18, 3369–3385, https://doi.org/10.5194/acp-18-3369-2018, 2018.

Li, J., Baier, B. C., Moore, F., Newberger, T., Wolter, S., Higgs, J., Dutton, G., Hintsa, E., Hall, B., and Sweeney, C.: A novel, cost-effective analytical method for measuring high-resolution vertical profiles of stratospheric trace gases using a gas chromatograph coupled with an electron capture detector, Atmos. Meas. Tech., 16, 2851–2863, https://doi.org/10.5194/amt-16-2851-2023, 2023.

Martinerie, P., Nourtier-Mazauric, E., Barnola, J.-M., Sturges, W. T., Worton, D. R., Atlas, E., Gohar, L. K., Shine, K. P., and Brasseur, G. P.: Long-lived halocarbon trends and budgets from atmospheric chemistry modelling constrained with measurements in polar firn, Atmos. Chem. Phys., 9, 3911–3934, https://doi.org/10.5194/acp-9-3911-2009, 2009.

Membrive, O., Crevoisier, C., Sweeney, C., Danis, F., Hertzog, A., Engel, A., Bönisch, H., and Picon, L.: AirCore-HR: a high-resolution column sampling to enhance the vertical description of CH_4 and CO_2, Atmos. Meas. Tech., 10, 2163—2181, https://doi.org/10.5194/amt-10-2163-2017, 2017.

Mrozek, D. J., van der Veen, C., Hofmann, M. E. G., Chen, H., Kivi, R., Heikkinen, P., and Röckmann, T.: Stratospheric Air Sub-sampler (SAS) and its application to analysis of $\Delta^{17}O(CO_2)$ from small air samples collected with an AirCore, Atmos. Meas. Tech., 9, 5607—5620, https://doi.org/10.5194/amt-9-5607-2016, 2016.

Pan, L. L., Atlas, E. L., Honomichl, S. B., Smith, W. P., Kinnison, D. E., Solomon, S., Santee, M. L., Saiz-Lopez, A., Laube, J. C., Wang, B., Ueyama, R., Bresch, J. F., Hornbrook, R. S., Apel, E. C., Hills, A. J., Treadaway, V., Smith, K., Schauffler, S., Donnelly, S., Hendershot, R., Lueb, R., Campos, T., Viciani, S., D'Amato, F., Bianchini, G., Barucci, M.,

Podolske, J. R., Iraci, L. T., Gurganus, C., Bui, P., Dean-Day, J. M., Millán, L., Ryoo, J.-M., Barletta, B., Koo, J.-H., Kim, J., Liang, Q., Randel, W. J., Thornberry, T., and Newman, P. A.: East Asian summer monsoon delivers large abundances of very short-lived organic chlorine substances to the lower stratosphere, P. Natl. Acad. Sci. USA, 121, e2318716121, https://doi.org/10.1073/pnas.2318716121, 2024.

Park, S., Western, L. M., Saito, T., Redington, A. L., Henne, S., Fang, X., Prinn, R. G., Manning, A. J., Montzka, S. A., Fraser, P. J., Ganesan, A. L., Harth, C. M., Kim, J., Krummel, P. B., Liang, Q., Mühle, J., O'Doherty, S., Park, H., Park, M.-K., Reimann, S., Salameh, P. K., Weiss, R. F., and Rigby, M.: A decline in emissions of CFC-11 and related chemicals from eastern China, Nature, 590, 433–437, https://doi.org/10.1038/s41586-021-03277-w, 2021.

Persson, C. and Leck, C.: Determination of reduced sulfur compounds in the atmosphere using a cotton scrubber for oxidant removal and gas chromatography with flame photometric detection, Anal. Chem., 66, 983–987, https://doi.org/10.1021/ac00079a009, 1994.

Ploeger, F., Gottschling, C., Griessbach, S., Grooß, J.-U., Guenther, G., Konopka, P., Müller, R., Riese, M., Stroh, F., Tao, M., Ungermann, J., Vogel, B., and von Hobe, M.: A potential vorticity-based determination of the transport barrier in the Asian summer monsoon anticyclone, Atmos. Chem. Phys., 15, 13145–13159, https://doi.org/10.5194/acp-15-13145-2015, 2015.

Ray, E. A., Moore, F. L., Elkins, J. W., Rosenlof, K. H., Laube, J. C., Röckmann, T., Marsh, D. R., and Andrews, A. E.: Quantification of the SF6 lifetime based on mesospheric loss measured in the stratospheric polar vortex, J. Geophys. Res.-Atmos., 122, 4626–4638, https://doi.org/10.1002/2016JD026198, 2017.

Ray, E. A., Moore, F. L., Garny, H., Hintsa, E. J., Hall, B. D., Dutton, G. S., Nance, D., Elkins, J. W., Wofsy, S. C., Pittman, J., Daube, B., Baier, B. C., Li, J., and Sweeney, C.: Age of air from in situ trace gas measurements: insights from a new technique, Atmos. Chem. Phys., 24, 12425–12445, https://doi.org/10.5194/acp-24-12425-2024, 2024.

Röckmann, T., Brass, M., Borchers, R., and Engel, A.: The isotopic composition of methane in the stratosphere: high-altitude balloon sample measurements, Atmos. Chem. Phys., 11, 13287–13304, https://doi.org/10.5194/acp-11-13287-2011, 2011.

Saunders, L. N., Walker, K. A., Stiller, G. P., von Clarmann, T., Haenel, F., Garny, H., Bönisch, H., Boone, C. D., Castillo, A. E., Engel, A., Laube, J. C., Linz, M., Ploeger, F., Plummer, D. A., Ray, E. A., and Sheese, P. E.: Age of air from ACE-FTS measurements of sulfur hexafluoride, Atmos. Chem. Phys., 25, 4185–4209, https://doi.org/10.5194/acp-25-4185-2025, 2025.

Say, D., Manning, A. J., Western, L. M., Young, D., Wisher, A., Rigby, M., Reimann, S., Vollmer, M. K., Maione, M., Arduini, J., Krummel, P. B., Mühle, J., Harth, C. M., Evans, B., Weiss, R. F., Prinn, R. G., and O'Doherty, S.: Global trends and European emissions of tetrafluoromethane (CF_4), hexafluoroethane (C_2F_6) and octafluoropropane (C_3F_8), Atmos. Chem. Phys., 21, 2149–2164, https://doi.org/10.5194/acp-21-2149-2021, 2021.

Schmidt, U., Kulessa, G., Klein, E., Röth, E.-P., Fabian, P., and Borchers, R.: Intercomparison of balloon-borne cryogenic whole air samplers during the MAP/GLOBUS 1983 campaign, Planet. Space Sci., 35, 647–656, 1987.

Schuck, T. J., Lefrancois, F., Gallmann, F., Wang, D., Jesswein, M., Hoker, J., Bönisch, H., and Engel, A.: Establishing long-term measurements of halocarbons at Taunus Observatory, Atmos. Chem. Phys., 18, 16553–16569, https://doi.org/10.5194/acp-18-16553-2018, 2018.

Schuck, T. J., Blank, A.-K., Rittmeier, E., Williams, J., Brenninkmeijer, C. A. M., Engel, A., and Zahn, A.: Stability of halocarbons in air samples stored in stainless- steel canisters, Atmos. Meas. Tech., 13, 73–84, https://doi.org/10.5194/amt-13-73-2020, 2020.

Schuck, T. J., Degen, J., Keber, T., Meixner, K., Wagenhäuser, T., Ghysels, M., Durry, G., Amarouche, N., Zanchetta, A., van Heuven, S., Chen, H., Laube, J. C., Baartman, S. L., van der Veen, C., Popa, M. E., and Engel, A.: Measurement report: Greenhouse gas profiles and age of air from the 2021 HEMERA-TWIN balloon launch, Atmos. Chem. Phys., 25, 4333–4348, https://doi.org/10.5194/acp-25-4333-2025, 2025.

Simmonds, P. G., Rigby, M., Manning, A. J., Park, S., Stanley, K. M., McCulloch, A., Henne, S., Graziosi, F., Maione, M., Arduini, J., Reimann, S., Vollmer, M. K., Mühle, J., O'Doherty, S., Young, D., Krummel, P. B., Fraser, P. J., Weiss, R. F., Salameh, P. K., Harth, C. M., Park, M.-K., Park, H., Arnold, T., Rennick, C., Steele, L. P., Mitrevski, B., Wang, R. H. J., and Prinn, R. G.: The increasing atmospheric burden of the greenhouse gas sulfur hexafluoride (SF_6), Atmos. Chem. Phys., 20, 7271–7290, https://doi.org/10.5194/acp-20-7271-2020, 2020.

Stanley, K. M., Say, D., Muhle, J., Harth, C. M., Krummel, P. B., Young, D., O'Doherty, S. J., Salameh, P. K., Simmonds, P. G., Weiss, R. F., Prinn, R. G., Fraser, P. J., and Rigby, M.: Increase in global emissions of HFC-23 despite near-total expected reductions, Nat. Commun., 11, 397, https://doi.org/10.1038/s41467-019-13899-4, 2020.

Stiller, G. P., von Clarmann, T., Haenel, F., Funke, B., Glatthor, N., Grabowski, U., Kellmann, S., Kiefer, M., Linden, A., Lossow, S., and López-Puertas, M.: Observed temporal evolution of global mean age of stratospheric air for the 2002 to 2010 period, Atmos. Chem. Phys., 12, 3311–3331, https://doi.org/10.5194/acp-12-3311-2012, 2012.

Tans, P.: Fill dynamics and sample mixing in the AirCore, Atmos. Meas. Tech., 15, 1903–1916, https://doi.org/10.5194/amt-15-1903-2022, 2022.

Umezawa, T., Sugawara, S., Hikichi, S., Morimoto, S., Saito, T., Krummel., P. B., Fraser, P. J., and Weiss, R. F.: New estimates of stratospheric age of air from halocarbon measurements of air samples collected by a balloon-borne cryogenic air sampler over Japan, ESS Open Archive [preprint], https://doi.org/10.22541/essoar.172108247.78209450/v1, 15 July 2024.

Voet, F., Ploeger, F., Laube, J., Preusse, P., Konopka, P., Grooß, J.-U., Ungermann, J., Sinnhuber, B.-M., Höpfner, M., Funke, B., Wetzel, G., Johansson, S., Stiller, G., Ray, E., and Hegglin, M. I.: On the estimation of stratospheric age of air from correlations of multiple trace gases, Atmos. Chem. Phys., 25, 3541–3565, https://doi.org/10.5194/acp-25-3541-2025, 2025.

Vogel, B., Günther, G., Müller, R., Grooß, J.-U., Afchine, A., Bozem, H., Hoor, P., Krämer, M., Müller, S., Riese, M., Rolf, C., Spelten, N., Stiller, G. P., Ungermann, J., and Zahn, A.: Long-range transport pathways of tropospheric source gases originating in Asia into the northern lower stratosphere during the Asian

monsoon season 2012, Atmos. Chem. Phys., 16, 15301–15325, https://doi.org/10.5194/acp-16-15301-2016, 2016.

Vogel, B., Müller, R., Günther, G., Spang, R., Hanumanthu, S., Li, D., Riese, M., and Stiller, G. P.: Lagrangian simulations of the transport of young air masses to the top of the Asian monsoon anticyclone and into the tropical pipe, Atmos. Chem. Phys., 19, 6007—6034, https://doi.org/10.5194/acp-19-6007-2019, 2019.

Volk, C. M., Elkins, J. W., Fahey, D. W., Dutton, G. S., Gilligan, J. M., Loewenstein, M., Podolske, J. R., Chan, K. R., and Gunson, M. R.: Evaluation of source gas lifetimes from stratospheric observations, J. Geophys. Res.-Atmos., 102, 25543–25564, https://doi.org/10.1029/97JD02215, 1997.

Vollmer, M. K., Mühle, J., Henne, S., Young, D., Rigby, M., Mitrevski, B., Park, S., Lunder, C. R., Rhee, T. S., Harth, C. M., Hill, M., Langenfelds, R. L., Guillevic, M., Schlauri, P. M., Hermansen, O., Arduini, J., Wang, R. H. J., Salameh, P. K., Maione, M., Krummel, P. B., Reimann, S., O'Doherty, S., Simmonds, P. G., Fraser, P. J., Prinn, R. G., Weiss, R. F., and Steele, L. P.: Unexpected nascent atmospheric emissions of three ozone-depleting hydrochlorofluorocarbons, P. Natl. Acad. Sci. USA, 118, e2010914118, https://doi.org/10.1073/pnas.2010914118, 2021.

Wagenhäuser, T., Engel, A., and Sitals, R.: Testing the altitude attribution and vertical resolution of AirCore measurements with a new spiking method, Atmos. Meas. Tech., 14, 3923—3934, https://doi.org/10.5194/amt-14-3923-2021, 2021.

Wagenhäuser, T., Engel, A., Bönisch, H., Ray, E., Garny, H., and Voet, F.: AtmosphericAngels/AoA from convolution: Software version as used in Garny et al. 2024, Version v1.0.0, Zenodo [data set], https://doi.org/10.5281/zenodo.11127613, 2024.

Weiss, R. F., Ravishankara, A. R., and Newman, P. A.: Huge gaps in detection networks plague emissions monitoring, Nature, 595, 491–493, https://doi.org/10.1038/d41586-021-01967-z, 2021.

Western, L. M., Redington, A. L., Manning, A. J., Trudinger, C. M., Hu, L., Henne, S., Fang, X., Kuijpers, L. J. M., Theodoridi, C., Godwin, D. S., Arduini, J., Dunse, B., Engel, A., Fraser, P. J., Harth, C. M., Krummel, P. B., Maione, M., Mühle, J., O'Doherty, S., Park, H., Park, S., Reimann, S., Salameh, P. K., Say, D., Schmidt, R., Schuck, T., Siso, C., Stanley, K. M., Vimont, I., Vollmer, M. K., Young, D., Prinn, R. G., Weiss, R. F., Montzka, S. A., and Rigby, M.: A renewed rise in global HCFC-141b emissions between 2017–2021, Atmos. Chem. Phys., 22, 9601–9616, https://doi.org/10.5194/acp-22-9601-2022, 2022.

Western, L. M., Vollmer, M. K., Krummel, P. B., Adcock, K. E., Fraser, P. J., Harth, C. M., Langenfelds, R. L., Montzka, S. A., Mühle, J., O'Doherty, S., Oram, D. E., Reimann, S., Rigby, M., Vimont, I., Weiss, R. F., Young, D., and Laube, J. C.: Global increase of ozone-depleting chlorofluorocarbons from 2010 to 2020, Nat. Geosci., 16, 309–313, https://doi.org/10.1038/s41561-023-01147-w, 2023.

WMO (World Meteorological Organization): Scientific Assessment of Ozone Depletion: 2022, WMO, Geneva, GAW Report No. 278, 509 pp., ISBN 978-9914-733-97-6, 2022.